J MATER SCI **41** (2006) 2631–2639

Model for kink-like deformation in CoTi single crystals

L. ZHANG*, M. L. JENKINS, G. TAYLOR†
Department of Materials, Oxford University, Parks Road, Oxford, OX1 3PH, UK

Published online: 17 April 2006

Single crystals of the B2 CoTi intermetallic compound were deformed in compression at temperatures between room temperature and 1000 K. The orientation was about 10° off the [001] cube axis. For B2 compounds with 'strong' AB bonding, the slip dislocations are often ⟨100⟩ type gliding on {110} planes although ⟨110⟩ and ⟨111⟩ slip cannot be ruled out especially when, as in this case, the Schmid factors for ⟨100⟩ glide are very small. In the lower half of the temperature range, deformation progressed by a series of load drops which manifests itself as coarse bands formed at intervals along the gauge length. The bands are roughly parallel to the (001) plane but it is concluded that the slip planes are {110} and that the kink-like behaviour is due to the formation of twist boundaries. A model for this behaviour is presented which is based on a pole mechanism and the glide of ⟨100⟩ dislocations.

1. Introduction

CoTi crystallises in the B2 structure which differs from the bcc structure only in that the atoms occupying the body-centring positions are a different chemical species from the atoms at the corners of the unit cell; so formally the B2 is a simple cubic structure. In consequence, the smallest unit lattice vector is $a\langle 100\rangle$ followed by $a\langle 110\rangle$ and $a\langle 111\rangle$, $cp\ \frac{a}{2}\langle 111\rangle$ for bcc. On the other hand the plane with the closest packing is still {110} and since each plane contains equal numbers of A and B atoms adjacent planes are identical. CoTi is a Berthollide compound, stable up to the melting point and with a limited composition range, ∼46–51 at.% Ti, i.e. favouring the Co rich side of stoichiometry.

Although $a\langle 100\rangle$ is the smallest lattice vector, a pair of $a\langle 100\rangle$ type dislocations can react to form an $a\langle 110\rangle$ dislocation without a change in elastic strain energy according to the b^2 law. In fact combining all three variants of $a\langle 100\rangle$ leads to the formation of $a\langle 111\rangle$ dislocations again without change in elastic strain energy. However, since there is nothing binding the unit dislocations together, it is probably unlikely that $a\langle 110\rangle$ or $a\langle 111\rangle$ dislocations will be the main slip vector since a small imbalance in the forces on the component parts of a compound dislocation will assist the emission of an $a\langle 100\rangle$ dislocation. On the other hand, the $a\langle 111\rangle$ dislocation can be stabilised by dissociation into superpartials provided the anti-phase boundary (APB) energy is not large i.e.

$$a[111] \Rightarrow \frac{a}{2}[111] + \text{APB} + \frac{a}{2}[111]$$

In this reaction the elastic strain energy is reduced by 50%. The dissociation may take place on either {110} or {211} planes and this is probably what happens in β–brass and other Kurnakov type compounds. For Berthollide and Daltonide type compounds, the AB bond energies may be too large (compared with AA and BB bonds) for the dissociation to occur.

The need to use single crystals in deformation studies on CoTi is shown by an analysis of the possible slip systems in B2 compounds. If acting alone, only the ⟨111⟩ dislocations are able to satisfy the von Mises conditions for an arbitrary shape change although a combination of $a\langle 100\rangle$ and $a\langle 110\rangle$ slip dislocations will also meet these conditions. Even with a single crystal, there is a problem if the slip vector is restricted to ⟨100⟩ since a force applied along the cube direction results in zero resolved stress on all possible slip systems.

*Present Address: Department of Materials Science and Metallurgy, Cambridge University, Pembroke Street, Cambridge, CB3 2QZ, UK.
†Author to whom all correspondence should be addressed.
0022-2461
DOI: 10.1007/s10853-006-7826-7

Virtually all intermetallic compounds are brittle at ambient temperatures. In many cases this is attributed to the complex nature of the dislocation core leading to sessile configurations. An additional source of brittleness for B2 compounds may be extrinsic. Since the positions of the atoms are essentially identical with bcc metals and alloys, there is little reason to suppose that interstitial atoms will not play a similar role in the two structures. We may therefore expect to find dislocation locking (Cottrell locking), yield point drops and brittleness due to dissolved interstitials unless special measures are taken to remove them.

Previous work on the mechanical properties of CoTi has been sparse. The most extensive work was by Takasugi and co-workers with a series of papers published between 1988 and 1995 [1–4]. More recently there have been papers by Wittmann *et al*. [5, 6]. Preliminary work at Oxford [7] has not been published in the open literature. What these studies have shown is that CoTi is a B2 intermetallic that exhibits anomalous strengthening, though the peak-stress temperature is rather low at ∼600–700 K. The stress strain curves show some serrated flow in the range immediately below the peak-stress temperature. Warwick [7] also showed that using cobalt-rich off-stoichiometric compositions gave greatly increased yield/flow stresses; the anomaly is not suppressed but the graph is shifted along the stress axis by about 600 MPa for the addition of 2–3% excess cobalt. This is a much larger effect than the anomaly exhibited by the stoichiometric alloy. According to [8] the excess cobalt atoms form antisite defects occupying atomic positions on the Ti sublattice. The off-stoichiometric alloys are, however, extremely brittle.

Transmission electron microscopy (TEM) studies have shown that many of the dislocations present in CoTi have $a\langle 100\rangle$ type Burgers vectors probably gliding on {110} type planes. What is less clear is whether slip can take place by glide of $a\langle 110\rangle$ and/or $a\langle 111\rangle$ dislocations.

2. Experimental procedures

The intermetallic compound was made by two methods (a) combustion synthesis of mixed, compacted Co and Ti powders, (b) melting together appropriate quantities of bulk Co and 'iodide' Ti in a tungsten arc furnace. Growing single crystals of CoTi compounds is a very difficult process with a low success rate [9]. In the present work crystals were grown successfully only from the type (b) material and since the procedure is long and involved it will be the subject of a separate paper. In the final stage of crystal growth, a molten zone was traversed slowly along the length of a 6 mm diameter rod under high vacuum. The orientation of the crystal rods was determined by the X-ray, back-reflection Laue technique. The as-grown crystal rods were centreless ground to 3.1 mm diameter and annealed at ∼1000°C in high vacuum (2×10^{-6}mbar). Compression samples, right cylinders 8 mm long, were produced from the crystals and the cylindrical surfaces electropolished to a mirror finish to facilitate slip-line analysis after deformation.

Samples were deformed in compression at a strain rate of $1.25\times10^{-4}\,S^{-1}$ and at temperatures between 298 K and 973 K using an elastically stiff, integrated testing machine. The testing atmosphere was a rough vacuum (pressure $\sim4\times10^{-3}$ mbar) after flushing a few times with helium gas. The hot end of the testing rig was constructed from a molybdenum alloy (TZM) with anvils of stellite or alumina. The sample was heated indirectly by induction using a niobium susceptor. Thermocouples were used to measure and control the susceptor temperature and the sample temperature was determined using calibration charts prepared by Bird [10]. Transmission electron microscopy samples were made from crystals that had been compressed ∼2%. Slices >0.6 mm thick were cut using a spark erosion wire cutter, or more usually a wafer thin SiC slitting wheel, and then hand-ground on each side using fine grade SiC papers to a thickness of ∼200 μm. Foils were made by electropolishing the discs in a Struers Tenupol twin-jet unit until perforation. The electrolyte was 30% HNO_3 in methanol by volume and optimal conditions were 25 V, 1.0 A and a bath temperature of −25°C.

3. Results

The composition of the single crystals, as measured by quantitative electron-probe microanalysis using a JEOL JXA 8800 instrument, was very close to stoichiometric ∼49.95 at.% Co and 50.05 at.% Ti. In addition the levels of oxygen and nitrogen were measured by Timet UK Ltd using the inert gas fusion technique; these levels were 350 and 55 at.ppm respectively.

The orientation of the as-grown single crystal rods is shown in Fig. 1; it is about 9° from [001] and close to $[\bar{1}1\,10]$. Back-reflection Laue photographs taken on the cylindrical surface of the crystals grown in vacuo were excellent but it was not possible to obtain a spot pattern from a crystal with any other surface e.g. grains grown under argon, mechanically, chemically or electrochemically

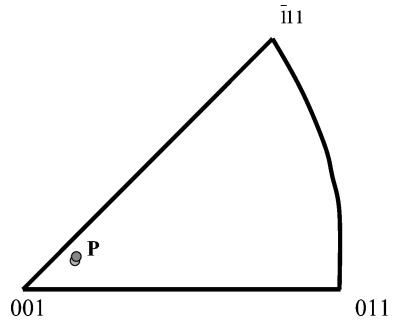

Figure 1 Orientation of the as-grown single crystal rods.

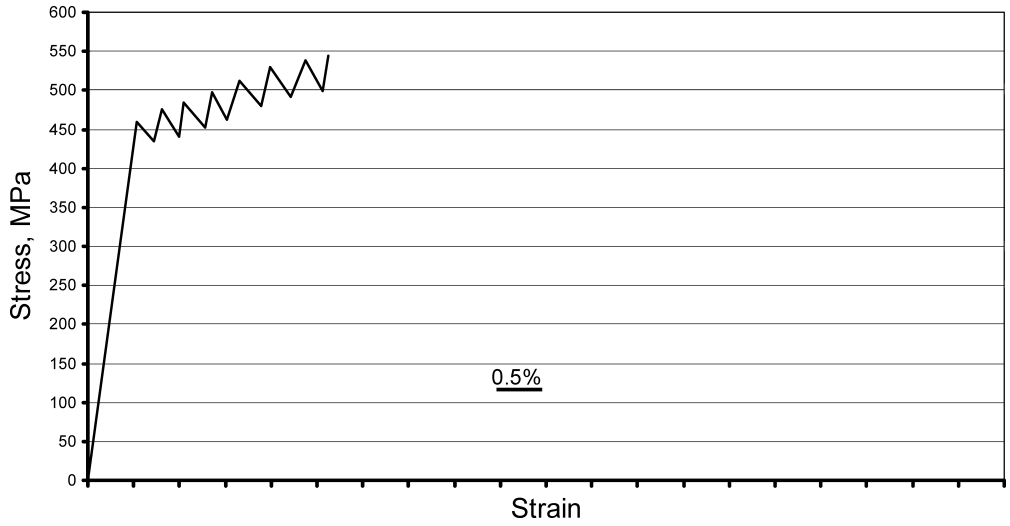

Figure 2 Stress vs. strain curve showing serrated flow, crystal deformed at a temperature of 473 K and a strain rate of 1.25×10^{-4} S^{-1}.

polished surfaces. In these cases the Laue photographs showed the usual background intensity but few if any spots. On the other hand electron diffraction did not seem to be affected adversely by different surface treatments. Provided the finish was optically smooth, diffraction patterns in TEM and EBSD mapping in the SEM were normal. It did mean, however, that it was not possible to check the orientations of individual samples before deformation nor align the crystal for cuttingslices with a specific crystallographic orientation after compression.

At intermediate temperatures, the stress-strain curves were heavily serrated. From the yield point, the deformation progressed by a series of load drops until the test was stopped. At 473 K, for example, the yield stress was ∼460 MPa and a plastic strain of 2% was achieved in 7 load drops each on average equivalent to ∼50 MPa, as shown in Fig. 2. There was no smooth deformation and no indication of plastic flow prior to the first load drop. The overall work-hardening rate was low. In comparison Takasugi *et al*. [2], using a similar orientation, found irregular small serrations and a high work-hardening rate.

After deformation, the sample surfaces were examined for slip lines using optical microscopy enhanced with Nomarski interference contrast and by scanning electron microscopy (SEM). The samples showed coarse slip bands visible to the naked eye. The bands were localised and distributed along the length of the sample; band normals made angles of 10–15° to the compression axis. The bands were best seen using SEM at low magnifications because of the large depth of field, as shown in Fig. 3. Within the coarsest bands there was a substructure in that the traces of individual slip 'lines' were not exactly parallel to each other but spread over a few degrees. With Nomarski interference contrast surface steps as small as 25 Å can be detected. The deformed crystals were mounted in a 1-circle goniometer which allowed 360° rotation about the compression axis so that the whole of the cylindrical surface could be examined. However, no normal slip lines could be seen on any of the samples. As a check on the technique, polycrystalline compression samples showed an abundance of fine slip lines corresponding to several different slip planes in each grain,after similar small strains.

Since normal fine-slip slip planes could not be identified, slices for TEM analysis were cut parallel to the deformation bands, perpendicular to the compression axis or across the deformation bands. Material within the coarse bands was extremely brittle or otherwise prone to fracture so despite careful grinding none reached a thickness suitable for electropolishing; consequently, no foils were obtained from slices that included the most highly deformed material.

From the subsequent electron diffraction patterns, slices cut parallel to the deformation bands produced foils that were close to (001) planes. The extensive Burgers vector analysis by TEM will be published elsewhere so only the conclusions will be included in this paper. Some foils contained very few dislocations so that the dislocation density was no higher than that observed in undeformed crystals, but mostly the density was suitable for easy Burgers vector analysis. The dislocations were imaged in brightfield under a wide range of two-beam conditions using reflections from the [001], ⟨110⟩ and ⟨111⟩ beam directions. Usually 14 or more images were recorded for each set of dislocations for Burgers vector and slip plane determination. In addition darkfield images were recorded usually under **g**/3**g** conditions. The analyses showed that the Burgers vectors of the dislocations were always ⟨100⟩ type. No ⟨110⟩ or ⟨111⟩ dislocations were found. Nearly always the dislocations had a[100] and a[010] Burgers vectors; an example is shown in Fig. 4a with $\mathbf{g} = 1\bar{1}0$. Dislocations labelled A have

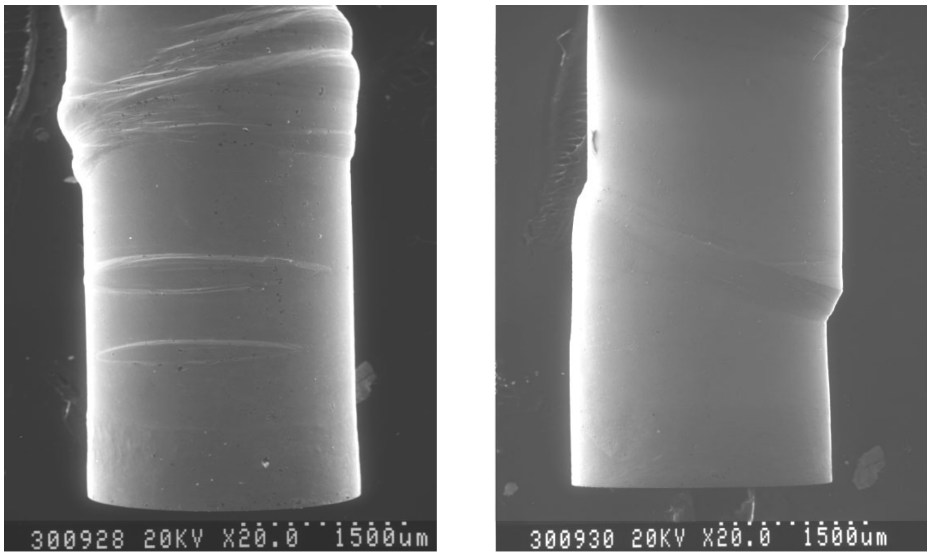

Figure 3 Low-magnification SEM images of compression samples showing coarse, kink-like bands after ∼2% deformation at 473 K and 573 K respectively.

[100] vectors and those labelled B [010]. Generally the dislocations were mixed character but with significant screw components. Although (001) is a possible glide plane for both types of dislocation it is not thought to be the slip plane. By tilting the foil so that the beam direction lies along [011] (Fig. 4b) or [111] (Fig. 4c), the dislocation images become much straighter. In Fig. 4c the a[100] dislocations lie along the [$\bar{2}$11] direction and the a[010] dislocations along [1$\bar{2}$1].

4. Discussion

Since ⟨100⟩, ⟨110⟩ and ⟨111⟩ slip directions have been proposed/observed for different B2 intermetallic compounds, it is important to establish the deformation modes in CoTi. The fact that the structure is stable up to the melting point and has a fairly narrow composition range suggests that CoTi should come into the category of ⟨100⟩ slip only. However, the NiAl B2 compound has similar phase characteristics to CoTi but it is possible to force ⟨111⟩ slip in this material. This is because when the direction of loading is along a cube axis the resolved shear stress on slip systems incorporating a⟨100⟩ dislocations is nominally zero. In the case of NiAl, for example, ⟨111⟩ slip takes place only if the temperature is low; the yield stress for ⟨111⟩ slip is extremely large ∼2 GPa, see for example [11] . Crystals of B2 NiAl do not appear to show the yield stress anomaly; however [001] oriented crystals do deform by kinking on [001] planes if the temperature is above ∼300 K [12, 13]. However the kinked volumes were found to be adjacent to the anvils (where there are additional frictional constraints), similar to earlier work on CoTi [2] but unlike the present results where the bands are distributed at intervals along the length of the sample.

Since the orientation of the crystals deformed in this work is close to [001], they are ideal for checking for slip by either a⟨110⟩ or a⟨111⟩ dislocations. Dislocations with ⟨111⟩ Burgers vectors may slip on either {211} planes or {110} planes, according to extensive work on bcc crystals as well as more limited information on B2. Dislocations with ⟨110⟩ Burgers vectors are expected to glide on {110} planes. Looking at the most favourable systems, i.e. [$\bar{1}$11](1$\bar{1}$2), [111]($\bar{1}$01)] and [$\bar{1}$01](101), the Schmid factors are 0.4987, 0.4492 and 0.4867 respectively, and the next most favourably oriented systems of the same types also have Schmid factors close to these values because the crystal orientation is close to a double-glide boundary. These should be compared to Schmid factors for a⟨100⟩ dislocations with values between 0.063 and 0.137 (see Table I) for the six most highly stressed slip systems assuming glide is possible on {100} and {110} type planes. It may be argued that slip on {211} planes is unlikely in compression because shear is in the anti-twinning sense, (cf bcc metals). However, NiAl with [001] orientation has shown {211} slip though at very low temperatures [11]. The resolved stress available for glide of a⟨111⟩ and a⟨110⟩ dislocations is at least ∼4× as high as that for ⟨100⟩ glide. So, since only ⟨100⟩ dislocations have been observed for this orientation, the likelihood of slip by ⟨111⟩ or ⟨110⟩ dislocations for any orientation in stoichiometric CoTi must be very low. Indeed our tests at a higher strain rate shattered the samples withoutdetectable plastic strain.

Having established that slip occurs by glide of a⟨100⟩ type dislocations and that for this orientation the dominant

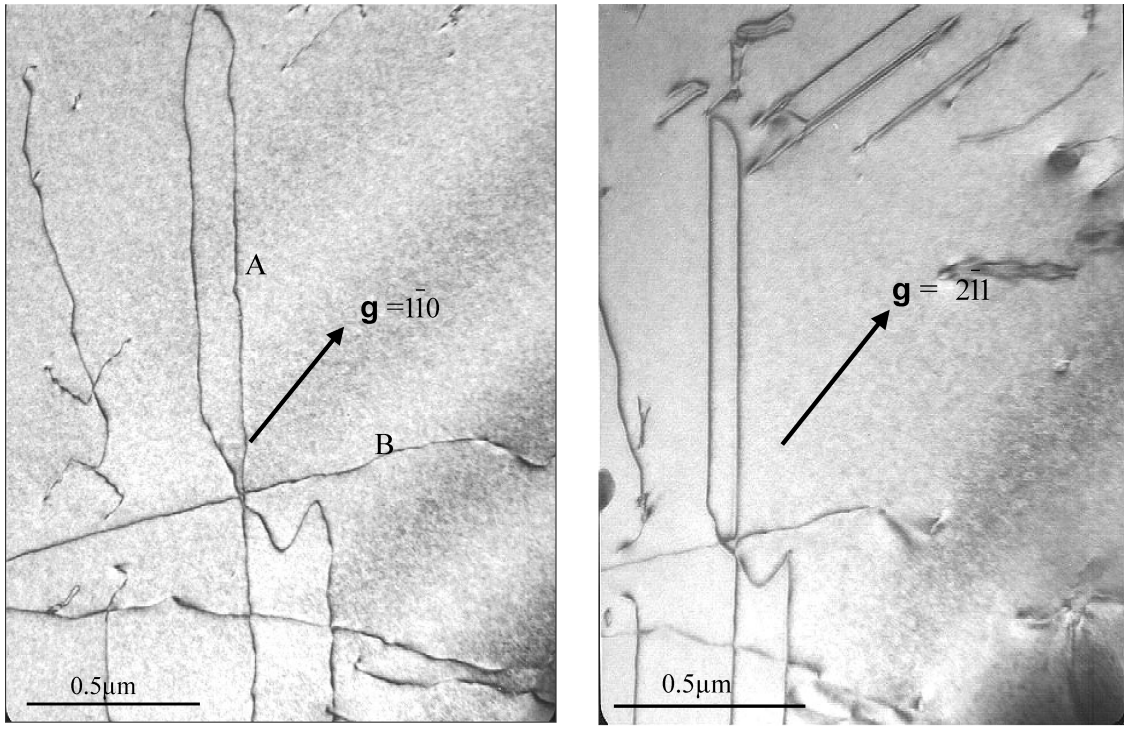

B = 001
(a)

B = 011
(b)

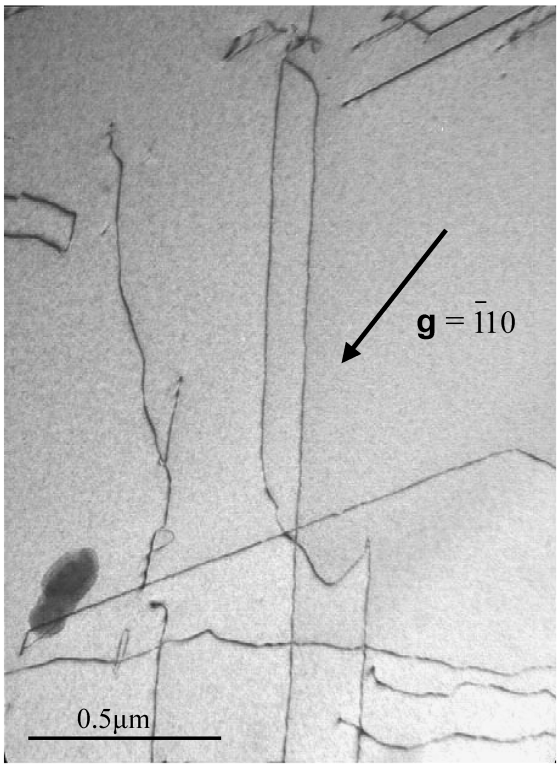

B = 111
(c)

Figure 4 Example of dislocations in foils cut parallel to the coarse deformation bands; the Burgers vectors are a[100] (labelled A) and a[010] (B) in Fig. 4a. Both sets appear bowed when viewed in the (001) projection (a) but are very much straighter when the foil is tilted so that the (0$\bar{1}$1) and ($\bar{1}$01) planes are perpendicular to the field of view, (b) and (c).

Burgers vectors are [100] and [010], the question of slip plane has to be considered. The surface markings, which can be seen with the naked eye and are shown in Fig. 3, make a small angle to the compression face of the crystal. The angle is not precise but varies from ∼10–15°. This means the plane may be close to (001); it is not possible to be sure because of the problems experienced getting Laue photographs from the test pieces. However, when loaded into the TEM and set to zero tilt, foils from samples cut approximately parallel to the coarse slip lines were close to showing the [001] beam direction pattern. (This is not the most accurate way of determining foil orientation but is the best we could do in the circumstances) Since there were no fine slip lines visible on the samples, it is tempting to conclude that (001) is the slip plane, particularly as it is a possible slip plane for both a[100] and a[010] dislocations. However, the TEM evidence is strongly against this conclusion. Looking again at Fig. 4 (and this was true for many other micrographs), it may be seen that the [100] dislocations appear pinned and bowed when the plane of view is (001). When the foil was tilted so that the beam direction is along [011] or [111], the long segments were almost perfectly straight. The only way a bowed dislocation can appear straight is if the plane of bowing (the slip plane) is viewed edge on. This means the direction perpendicular to the straight dislocation segments is the pole of the slip plane, and for the [100] dislocations the slip plane is $(0\bar{1}1)$. Similar analysis for the [010] dislocations in Fig. 4 shows that the slip plane for these dislocations is $(\bar{1}01)$. (It is possible that the slip plane for a[100] dislocations is (011) rather than $(0\bar{1}1)$ and for a[010] dislocations, (101) rather than $(\bar{1}01)$; distinguishing between them relies on the foil being perpendicular to the beam direction at the start of the tilting experiments since the only way of identifying which of the 4⟨111⟩ zones or which of the 4 nearest ⟨110⟩ zones is being used, is by noting the angle of tilt on the goniometer stage. However, because of the symmetry of the crystal orientation, this does not materially affect the conclusion, just that the Schmid factor for [100](011) slip is somewhat larger than for [100]$(0\bar{1}1)$,though both are small.)

5. Model for kinking

Since it is concluded that the slip plane in CoTi at low temperatures (i.e. below the peak-stress temperature) is {110}, it is necessary to explain the lack of {110} slip traces and the formation of coarse bands roughly parallel to (001) planes. Externally the bands have some of the characteristics of kinks and if formed rapidly could produce the load drops that give rise to the 40–50 MPa serrations observed on the stress-strain curves. Kink bands are usually associated with edge dislocations forming, in effect, two large equal and opposite tilt boundaries. In the present work, several slices for TEM were cut approximately perpendicular to the bands to try to ensure that a boundary appeared in the thin part of the foil. However, these slices turned out to be exceptionally fragile and fractured during the fine-grinding on Si carbide papers so that none of them reached even the electropolishing stage. There was insufficient crystal for this part of the work to be repeated.

TABLE I Schmid factors for ⟨100⟩ slip on {110} or {100} planes in CoTi crystals shown in Fig. 1. Angles between compression axis and cube axes, [100], [010] and [001] are 85.4°, 83.0° and 8.5° respectively

[100]		[010]		[001]	
(011)	0.063	(101)	0.079	(110)	0.026
$(0\bar{1}1)$	0.049	$(\bar{1}01)$	0.093	$(\bar{1}10)$	0.137
(010)	0.0098	(100)	0.0098	(100)	0.079
(001)	0.079	(001)	0.121	(010)	0.121

However, considering a loop with a[100] Burgers vector expanding on the $(0\bar{1}1)$ slip plane (or (011) slip plane), the edge segments make an angle of ∼45° to the compression axis, whereas the screws are almost perpendicular. The screw segments will also lie in a (001) plane because [100] is the zone axis for (001) and $(0\bar{1}1)$ planes. The operation of a Frank-Read type source will produce a set of loops in a single $(0\bar{1}1)$ plane in which the edge and screw segments will form classic pile-ups if they reach a barrier but otherwise the edge dislocations will escape to the surface of the crystal giving distinct slip lines parallel to the traces of the $(0\bar{1}1)$ slip plane at ∼45° to the crystal axis. In order for the slip lines to be invisible, the deformation must be homogeneous, or nearly so. Homogeneous slip is a characteristic of deformation twinning and early models of twin growth were based on pole mechanisms [14, 15]. The pole dislocation must be approximately perpendicular to the plane of shear and the glide dislocation rotates around the pole climbing onto a new plane for each revolution. For the present case, this means the pole dislocation must have a screw component perpendicular to the slip plane and equal to the interplanar spacing or a multiple of it. The a[001] screw dislocation is suitable. Lying along the [001] direction it makes an angle of 45° to the $(0\bar{1}1)$ plane normal so the perpendicular component is $a[001]\times\cos 45^\circ = \frac{1}{2}a\sqrt{2}$. The interplanar spacing of {110} planes in cubic crystals, $d_{110} = \frac{1}{2}a\sqrt{2}$ which matches the step from the pole. In fact any mixed character [001] dislocation lying approximately perpendicular to the $(0\bar{1}1)$ planes may act as the pole, since this will also provide the required step per revolution.

The operation of the pole mechanism will produce homogeneous shear but if all the screws stop after gliding an appropriate distance from the pole they will form a dense array on (001) with a very large shear. A second array is needed to cancel the shear from the first and in doing so rotate the two parts of the crystal on either side of the (001) plane, forming a twist boundary.

The second array can be provided in the same way by a[010] dislocations gliding on $(\bar{1}01)$ (or (101)) planes. Again the pole dislocation can be an a[001] pure screw

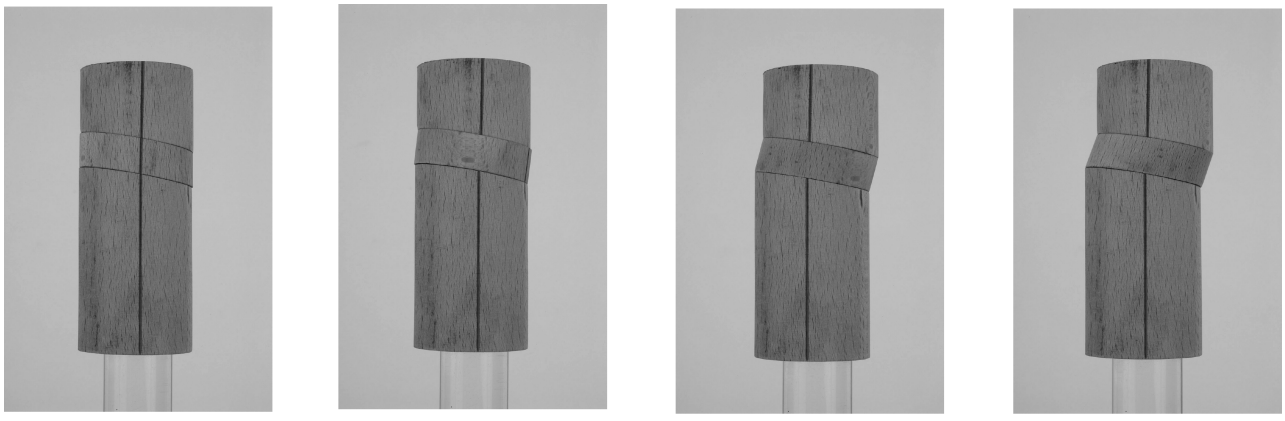

Figure 5 Wooden model showing the effect of a pair of twist boundaries on the external shape of a compression sample. The central section is rotated 60, 120 or 180° in (b), (c) and (d) respectively; the appearance depends also on camera angle.

or a mixed [001] dislocation roughly perpendicular to the $(\bar{1}01)$ planes. The common plane for the $a[100]$ and $a[010]$ dislocation arrays is, of course, (001) so this will be the plane containing the twist boundary. For each operation two boundaries will form with twists in opposite senses so, if each boundary is able to cover the cross section of the sample, the slice of crystal between the two twist boundaries will be rotated with respect to the rest of the crystal. An advantage of the B2 structure is that the two sets of $\langle 100 \rangle$ dislocations forming the twist boundaries are exactly perpendicular to each other so there should be no residual long-range stress, unlike most twist boundaries in fcc and bcc crystals. The amount of rotation provided by a twist boundary depends on the density of dislocations in each array. The angle of twist θ, is given by

$$\sin\left(\frac{\theta}{2}\right) = \frac{b}{2S}$$

where b is the magnitude of the Burgers vector and S the spacing of the dislocations. In the present model, the spacing of the {110} slip planes is $\frac{1}{2}a\sqrt{2}$ which will give a spacing between screws on the $(0\bar{0}1)$ planes of a. Since b is also equal to a, the angle of twist will be 60°. This is a very large angle for a dislocation based boundary and a little larger than the minimum energy twistboundary configuration of 53° proposed on the basis of the coincidence site lattice (CSL) model with $\Sigma = 5$.

A wooden model was constructed in which a slice cut at 10° to the compression face could be rotated various amounts to represent the pair of twist boundaries and their effect on the shape of the crystal sample. Figs 5a–d shows photographs of the wooden model taken for rotations of 0°, 60°, 120° and 180° respectively. (The appearance of the model was also dependent on the viewing (camera) angle). The larger angles may represent slices containing additional twist boundaries. These photographs may be compared with the SEM images of the kinked samples, shown in Fig. 3. It is clear that a model twist boundary can account visually for the changes that were observed macroscopically in the deformed crystals.

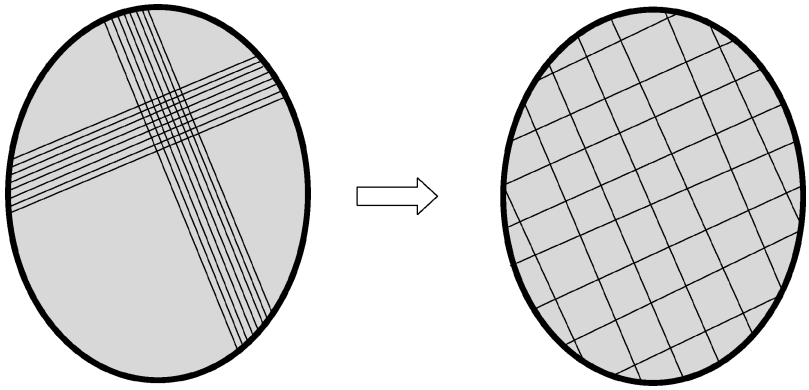

Figure 6 Diagram showing how two sets of screw dislocations may spread in the common plane increasing the area of twist boundary and at the same time reducing the angle of twist.

Smaller-angle twist boundaries may also be formed if the arrays are able to move in the (001) plane as shown in Fig. 6. Even though it is not a normal slip plane, (001) is a geometrically possible slip plane for both $a\langle 100\rangle$ and $a\langle 010\rangle$ dislocations. Allowing the edge components to escape through the crystal surface leaves two sets of long screws running across the (001) plane; but the length of the pole dislocation will limit the number of screws produced in each set. Only where the two sets cross each other will the stress fields be cancelled and the twist boundary formed. Outside this area, each set of screws will be subject to very large mutually repulsive forces from other dislocations within the same set. This may cause each set to spread in the (001) plane, increasing the area of the twist boundary whilst at the same time reducing the angle of twist.

In view of the above, it was decided to look again at the foils that had been prepared from slices cut approximately perpendicular to the compression axis and which also may have crossed a kink band. Although the density of screws that would give rise to a twist angle of 60° is much too large for the dislocations to be seen individually, it was still hoped to find evidence of twist boundaries. In a foil from a crystal deformed at 373 K, a substantial twist boundary was found in the thicker parts of the foil. Part of this is shown as a composite in Fig. 7. The projected width of the boundary varied from about 6–8 μm as the foil thickened and it was followed over ~60 μm. Burgers vector analysis showed that [100] screws and [010] screws make angles of 40° and 50° with the visible edge of the boundary in the foil. More of a surprise were another two sets of dislocations in the boundary, one set running approximately parallel to the long edge of theboundary and the other perpendicular to it. Burgers vector analysis showed that these dislocations were consistent with being [110] and $[\bar{1}10]$ screws respectively. The contrast, however was a little different from normal and the dislocations looked very straight but that may be connected with the high density. Alternatively, the cores may be extended on the appropriate {110} plane i.e. $(\bar{1}10)$ for $a[110]$ dislocations and (110) for $a[\bar{1}10]$. Spreading on the {110} could be promoted by a possible dissociation into superpartials, for example on the $(\bar{1}10)$ plane

$$a[110] \Rightarrow \frac{a}{2}[111] + \frac{a}{2}[11\bar{1}]$$

$$b^2 \qquad 2a^2 \Rightarrow 3\frac{a^2}{4} + 3\frac{a^2}{4}$$

However the separation is likely to be very small as the driving force is not large and the combined image behaves like $a[110]$; it is aided in the latter respect by the $(\bar{1}10)$ planes being perpendicular to the viewing plane so the images of any partials are on top of each other.

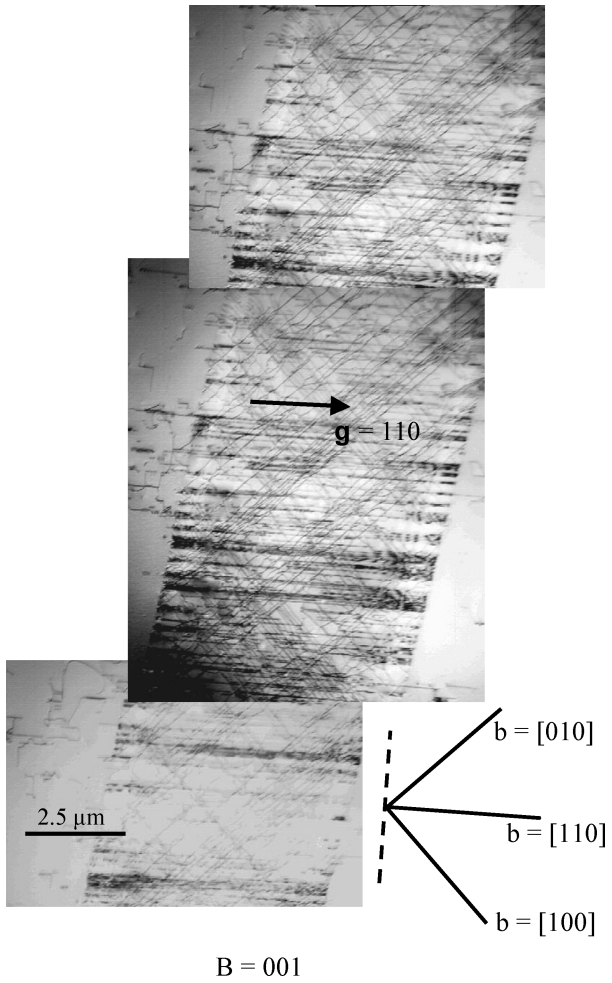

Figure 7 Dislocations forming part of a twist boundary in a crystal deformed at 373 K. The image was taken from a fairly thick part of the foil and has 4 sets of screw dislocations lying along [100], [110], [010] and $[\bar{1}10]$ directions. The broken line shows the orientation of the $[\bar{1}10]$ screws which are invisible in the 110 reflection.

An analogous argument applies to the $a[\bar{1}10]$ dislocation dissociating onto the (110) plane.

Since $\langle 110\rangle$ glide dislocations were not observed elsewhere in the foils, it may be the case that these dislocations were formed *in situ* from reactions between [100] and [010] dislocations since the (001) plane is common to all 4 dislocations e.g.

$$a[100] + a[010] \Rightarrow a[110]$$

There is no driving force for this reaction from the elastic strain energy because $\Sigma b^2 = 0$. Both $\langle 110\rangle$ screws can be derived from the same pair of $\langle 100\rangle$ dislocations, as shown in Fig. 8. The $[0\bar{1}0]$ dislocation in (b) is physically identical with the [010] dislocation shown in (a) because both the line direction and the Burgers vector have been reversed. This was done so that the resultant line directions in (b) were the same for both reactants.

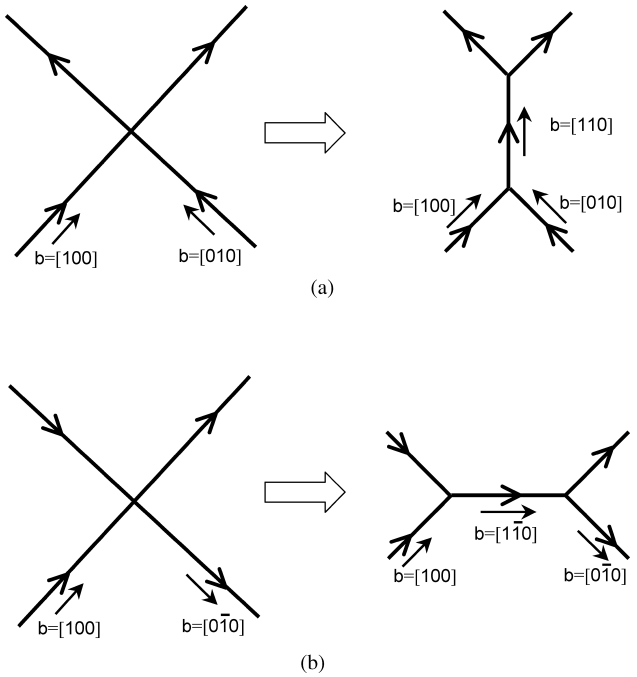

Figure 8 Schematic showing the formation of $a\langle 110\rangle$ dislocations from $a\langle 100\rangle$ type.

Since there is no reduction in elastic strain energy by the formation of $\langle 110\rangle$ screws, the driving force may be the reduction in core energy. For any large-angle twist boundary the cores in each array are overlapping because the dislocations are so close. With this reaction the total length of dislocation core is reduced because two dislocations are replaced by one. In addition, the core material is redistributed along new directions at 45° to the cores of the reactants. There may also be a contribution from anisotropic elasticity but this will depend on the specific elastic constants of CoTi which are not known; this contributioncould go either way.

6. Conclusions

The question of kinking and the accompanying load drops may be answered by this model. Deformation twins usually form very rapidly so if a pole mechanism is applicable for twin growth then it may also provide rapid deformation here. The fact that the axial load (stress) is very large compared with the resolved shear stress because of the small Schmid factor probably adds to the likelihood of instability. At orientations for which the Schmid factor is close to the maximum for $\langle 100\rangle\{110\}$ slip e.g. near to [011] and [111], it was shown [2] that the critical resolved shear stress (CRSS) was in the range 30–50 MPa at the intermediate minimum; the temperature of the minimum varied somewhat with crystal composition and orientation, in the range 300–473 K. In this work, the intermediate yield stress minimum occurred at 373 K for both samples and resolving on to the most favourably oriented $\langle 110\rangle$ type slip planes, the corresponding CRSS values are 28.8 and 19.5 MPa for [010]($\bar{1}$01) and [100](011) slip respectively.

Acknowledgments

The authors would like to thank Professor Yuangsheng Yang (Institute for Metal Research, China) for the gift of pure titanium and Professor G. D. W. Smith for laboratory facilities. L. Zhang would like to thank the University of Oxford for financial support.

References

1. T. TAKASUGI and O. IZUMI, *J. Mater. Sci.* **23** (1988) 1265.
2. T. TAKASUGI, K. TSUIAKI, O. IZUMI and S. ONO, *Phil. Mag.* **A61** (1990) 785.
3. T. TAKASUGI, M. YOSHIDA and T. KAWABATA, *ibid.* **A65** (1992) 29.
4. T. TAKASUGI, M. YOSHIDA, S. HANADA and D. SHINDO, *ibid.* **A71** (1995) 347.
5. M. WITTMANN, I. BAKER and N. D. EVANS, *Mater. Res. Soc. Symp. Proc.* **646** (2001) N3.5.1.
6. M. WITTMANN and I. BAKER, *Mater. Sci. Eng.* **A329–331** (2002) 206.
7. J. WARWICK, Part II thesis (1995), Oxford University.
8. T. TAKASUGI and O. IZUMI, *Phys. Stat. Sol. (a)* **102** (1987) 697.
9. Personal communication from Takasugi to Warwick (1995).
10. N. BIRD, D. Phil. thesis (1998), Oxford University
11. Y. Q. SUN and G. TAYLOR, in Intermetallic compounds for high temperature structural applications, edited by M. Yamaguchi and H Fukutomi 1230 (Japan SAMPE, Tokyo 1993).
12. R. D. FIELD, D. F. LAHRMAN and R. DAROLIA, *Acta Metall. Mater.* **39** (1991) 2951.
13. D. B. MIRACLE, *ibid.* **41** (1993) 649.
14. A. H. COTTRELL and B. A. BILBY, *Phil. Mag.* **42** (1951) 573.
15. N. THOMPSON and D. J. MILLARD, *ibid.* **43** (1953) 422.